Int. J. Heat Mass Transfer. Vol. 27, No. 9, pp. 1649–1657, 1984
Printed in Great Britain

0017–9310/84 $3.00 + 0.00

Heat exchanger situated downstream of a right-angle bend

E. M. SPARROW and Y. S. BERMAN
Department of Mechanical Engineering, University of Minnesota, Minneapolis, MN 55455, U.S.A.

(*Received* 9 *November* 1983)

Abstract—Heat transfer, pressure drop, and flow visualization experiments were performed for a tube-bank-type crossflow heat exchanger situated downstream of a right-angle bend. The heat exchanger was housed in a duct of square cross section, and the L-shaped duct which delivered the airflow to the tube bank inlet was of identical cross section. Two geometrical parameters were varied during the course of the experiments: (1) the distance between the bend and the tube bank inlet and (2) the orientation of the plane of the bend with respect to the axes of the tubes in the bank (either parallel or perpendicular to the axes). The Reynolds number was varied over nearly an order of magnitude. For each geometry and Reynolds number, per-tube heat transfer coefficients were determined at each relevant tube site in the array. It was found that the presence of the right-angle bend did not have a major effect on the heat transfer characteristics of the tube bank. Bend-related enhancements in the 10–15% range were encountered at individual tubes in the initial rows, but the row-average enhancements were smaller. Intra-row nonuniformities occurred for the perpendicular orientation but not for the parallel orientation. The system pressure drop (from delivery duct inlet to tube bank exit) was even less sensitive to the geometrical parameters than the per-tube heat transfer.

INTRODUCTION

IN HEAT exchanger installations, it is not uncommon that a right-angle bend is situated upstream of the inlet face of the exchanger. It is known that such a bend introduces nonuniformities in the velocity distribution, with the flow packing to the outside of the bend. In addition, the bend creates a secondary flow in the form of corkscrew-like vortices which are superposed on the main flow. Thus, the presence of the bend causes the flow that is presented to the inlet of the heat exchanger to be both nonuniformly distributed and nonunidirectional. The extent to which these nonidealities exist at the exchanger inlet depends on the distance between the bend and the inlet.

The research reported here is concerned with a tube-bank-type crossflow heat exchanger to which the crossflow fluid is delivered via a right-angle bend. Two orientations of the bend with respect to the tube bank were investigated. In one, the plane formed by the L-shaped delivery duct which contains the bend was oriented perpendicular to the axes of the tubes in the bank. On the other hand, in the other orientation, the plane of the L-shaped duct was parallel to the tube axes. These two orientations yield markedly different inlet-face flow patterns. In particular, the vortices spawned by the bend are oriented differently with respect to the tube axes, and the flow nonuniformity is differently distributed.

For each of the two orientations, the distance between the bend and the inlet was varied parametrically. Three distances were used, so that a total of six different configurations were investigated. For each configuration, experiments were performed for two Reynolds numbers which spanned nearly an order of magnitude.

For each case (given orientation, bend-to-inlet distance, and Reynolds number), per-tube Nusselt numbers were determined for each tube of the bank. Axial pressure distributions were also measured for each case, and friction factors, based on the pressure drop per row, were deduced. In addition, a flow visualization study, performed with the oil–lampblack technique, was undertaken with the aim of observing alterations in the fluid flow pattern in the heat exchanger due to the presence of the bend.

Despite the realization of the potential importance of inlet-section fluid flow maldistributions on heat exchanger performance [1], there appears to be very little relevant experimental work in the literature. As part of a long-range research program, of which the present paper describes the final phase, the authors have investigated maldistributions caused by partial cross-sectional blockages and abrupt enlargements [2, 3]. Computational models based on hypothesized (and unverified) distributions of the heat transfer coefficient have been proposed to estimate the effects of flow maldistribution [4–7]. These hypotheses include local application of heat transfer coefficients for nonmaldistributed flows and a power-law relation between the transfer coefficient and the mass velocity.

THE EXPERIMENTS

It was highly advantageous to carry out the research by means of mass transfer experiments. The per-tube Sherwood numbers (dimensionless mass transfer coefficients) determined from such experiments can be converted to per-tube Nusselt numbers using the well-established analogy between heat and mass transfer.

NOMENCLATURE

A_{min}	minimum free flow area between tubes	Sh_{fd}	fully developed per-tube Sherwood number
A_w	surface area of a tube	S	side of duct
D	tube diameter	S_L	longitudinal pitch
$\mathscr{D}$	diffusion coefficient	S_T	transverse pitch
f_{fd}	fully developed friction factor, $\Delta p_{row}/\frac{1}{2}\rho V^2$	V	velocity at minimum free flow area in bank
K	per-tube mass transfer coefficient, equation (1)	$\dot{w}$	mass flow rate
L^*	distance between bend and tube bank inlet	X	coordinate along duct centerline.
ΔM	change in mass during data run		
p	pressure	Greek symbols	
p_{atm}	ambient pressure	μ	viscosity
Δp_{row}	fully developed per-row pressure drop	ν	kinematic viscosity
Δp_{tot}	pressure drop for flow circuit	ρ	air density
Re	Reynolds number, $(\dot{w}/A_{min})D/\mu$	ρ_{nw}	naphthalene vapor density at tube surface
Sc	Schmidt number, $\nu/\mathscr{D}$	ρ_{nb}	naphthalene vapor density in bulk flow
Sh	per-tube Sherwood number, $KD/\mathscr{D}$	τ	duration of data run.

The mass transfer experiments were performed utilizing the naphthalene sublimation technique.

In the execution of the mass transfer experiments, an approach was adopted which is frequently used in experimental work on heat transfer in tube banks. In that approach, only one of the tubes in the bank is heated during a given data run, and the heated tube is positioned at different sites in the bank during different data runs. Similarly, in the present experiments, only one mass-transfer-active tube was used in each data run. However, for each case (given orientation, bend-to-inlet distance, and Reynolds number), sufficient runs were made to enable the active tube to be positioned at all relevant sites in the array.

Experimental apparatus

A schematic, pictorial view of the experimental apparatus is presented in Fig. 1. As seen there, an L-shaped duct (the delivery duct) conveys air drawn from the laboratory room to the test section, which houses a model of a tube-bank-type crossflow heat exchanger. The delivery duct and the test section are both of square cross section with side S. After traversing the test section, the air passes through a redevelopment length (also of $S \times S$ cross section) and is then ducted to a flowmeter (calibrated rotameter), control valve, and blower. The blower was situated in a service corridor outside the laboratory. The compression-heated, naphthalene-laden discharge of the blower was vented outside the building. Operation of the apparatus in the suction mode assured that the air delivered to the test section was free of naphthalene vapor.

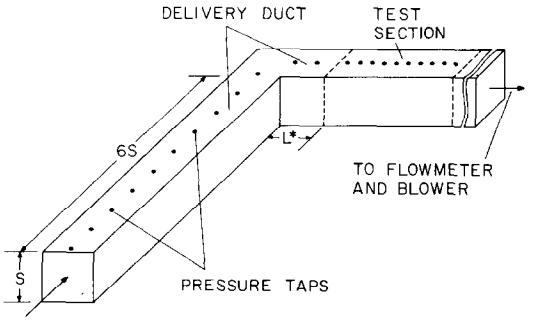

FIG. 1. Pictorial view of the experimental apparatus.

The portion of the L-shaped delivery duct situated upstream of the bend had a length equal to $6S$, and this length was fixed throughout the experiments. On the other hand, the length of the delivery duct downstream of the bend was one of the key parameters of the research. This length is designated as L^* in Fig. 1. The L^*/S values used during the research were 0.8, 2.5, and 4.5, with 0.8 being the smallest value consistent with the flanges and screw fittings that were used to connect the delivery duct to the test section.

In the execution of the research, the experiments for the $L^*/S = 4.5$ case (largest L^*) were carried out first. When these experiments were concluded, a portion of the downstream end of the delivery duct was cut off, leaving $L^*/S = 2.5$. Similarly, when the $L^*/S = 2.5$ case was completed, the duct was further cut to yield the $L^*/S = 0.8$ case.

As was noted earlier, two orientations of the bend with respect to the tube bank were investigated. These orientations are shown in Figs. 2 and 3. In Fig. 2, the plane of the L-shaped delivery duct is seen to be perpendicular to the axes of the tubes in the heat exchanger. This arrangement will hereafter be termed the perpendicular orientation. Figure 3 shows the parallel orientation wherein the plane of the L-shaped duct is parallel to the axes of the tubes.

Figure 2 also serves to illustrate the layout of the array. The tubes are seen to be on equilateral-triangular centers ($S_L/S_T = \sqrt{3}/2$), with $S_T/D = 2$. There are six tubes in each row. In alternate rows, half tubes are positioned adjacent to the side walls in order to help

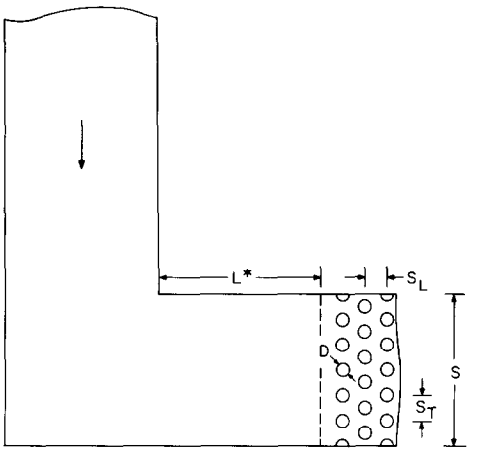

FIG. 2. Illustration of the perpendicular orientation.

approximate an array of infinite width. The experiments were performed with 15 rows of tubes. Downstream of the fifteenth row, the $S \times S$ cross section continues for a distance of about $10S$, at which point the transition from a square to a circular cross section occurs.

The heat exchanger tubes were modeled by solid cylinders fabricated from drill rod stock of diameter D. For those tubes which did not participate in the mass transfer process, the rod stock was used essentially as is, aside from cutting to the proper length (S) and buffing of the surface. The mass-transfer-active tubes were also fabricated from the same rod stock. To accommodate a thin naphthalene coating, the rods were machined to a slightly reduced diameter. The naphthalene was applied by a two-step process which first involved dipping the rod into molten naphthalene and then machining the solidified coating so as to obtain a hydrodynamically smooth surface of diameter D. A freshly coated rod was used for each data run. Further details of the coating procedure are given in ref. [2].

The actual physical dimensions of the apparatus may be specified via the side length S and the tube diameter D, whose values were 7.62 cm (3 in.) and 0.635 cm (0.250 in.).

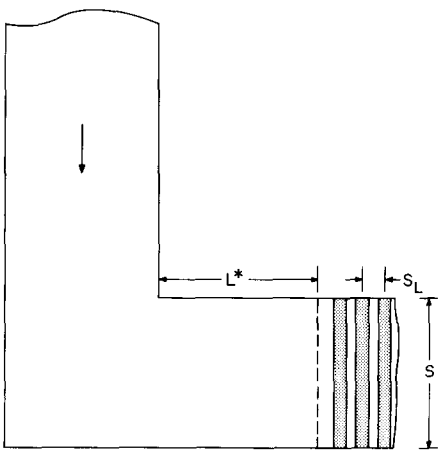

FIG. 3. Illustration of the parallel orientation.

Experimental procedure

In the execution of a data run, the primary objective is to determine the change of mass of the coated tube which results from the sublimation of the naphthalene during the run. Correspondingly, the mass of the coated tube is measured immediately before it is subjected to the airflow and immediately after the period of exposure. To accomplish these measurements, it is essential that the coated tube is able to be withdrawn from or installed in the test section with dispatch (i.e. in a few seconds). To this end, the upper wall of the test section was made removable and fitted with quick-acting clamps. The mass was measured by an ultra-precision electronic balance with a resolution of 10^{-5} g.

Each data run was preceded by a preparatory period during which the coated tube attained thermal equilibrium with the airflow. During this period, the tube was in place in the array but was covered with an impermeable Teflon jacket which suppressed mass transfer. The equilibration period was a prerequisite for the definition of the operating conditions of the experiment, especially since the vapor pressure of naphthalene (which drives the mass transfer) is sensitive to temperature.

Axial pressure distributions were measured in a set of experiments separate from the mass transfer experiments. The pressure tap locations are shown in Fig. 1. The pressure signals were measured with a Baratron pressure meter with a resolution of 0.001 Torr.

The flow visualization was performed using the oil–lampblack technique [8]. For this work, the floor of the test section was covered with white, self-adhering, plasticized contact paper in which holes were made to accommodate the lower ends of the tubes. Prior to the initiation of the airflow, the contact paper was brushed with a suitable mixture of lampblack powder and oil. When the airflow was activated and maintained, the mixture moved under the action of the fluid shear forces, yielding a pattern of lines which reflect the flow pattern adjacent to the floor of the test section.

RESULTS AND DISCUSSION

Data reduction

The evaluation of the per-tube mass transfer coefficient K involves the following quantities: (1) the change of mass ΔM during the data run, (2) the duration τ of the run, (3) the surface area A_w of the tube, (4) the naphthalene vapor density ρ_{nw} at the tube surface, and (5) the naphthalene vapor density ρ_{nb} in the airflow (b $\sim$ bulk). With these

$$K = (\Delta M/\tau A_w)/(\rho_{nw} - \rho_{nb}). \quad (1)$$

Among the foregoing, ΔM, τ, and A_w were directly measured, $\rho_{nb} = 0$, and ρ_{nw} was calculated from the vapor pressure–temperature equation for naphthalene [9] and the perfect gas law.

The per-tube Sherwood number may be defined as $Sh = KD/\mathscr{D}$, where $\mathscr{D}$ is the mass diffusion coefficient. By introducing the Schmidt number $Sc = \nu/\mathscr{D}$, the

diffusion coefficient can be eliminated, so that

$$Sh = (KD/v)Sc. \quad (2)$$

The Schmidt number for naphthalene diffusion in air is 2.5 [9].

The Sherwood number results will be parameterized by the Reynolds number. The velocity that appears in the Reynolds number was evaluated at the minimum free flow area A_{min}, so that $\rho V = \dot{w}/A_{min}$, where $\dot{w}$ is the flow rate of the air. In addition, the cylinder diameter D was used as the characteristic dimension. Thus

$$Re = (\dot{w}/A_{min})D/\mu. \quad (3)$$

In the present array, $A_{min} = \frac{1}{2}S^2$.

Mass (heat) transfer results

The Sherwood number results will be presented in terms of the ratio Sh/Sh_{fd}. In the ratio, the quantity Sh represents the per-tube Sherwood number at any site of interest in the array, while Sh_{fd} is the fully developed per-tube Sherwood number. Both Sh and Sh_{fd} correspond to the same Reynolds number. With regard to Sh_{fd}, it is known that an axially periodic flow pattern is established in a tube bank at sufficient distances from the inlet face. The periodic flow pattern gives rise to axially unchanging values of the per-tube Sherwood (or Nusselt) number, as was affirmed by the present experiments. The Sh_{fd} values measured here for Re = 1000 and 8600 are 30.45 and 117.3, respectively.

The Sherwood number ratios are presented in Figs. 4–6. Each of these figures is a plan-view layout of the array. Adjacent to each tube (excluding the half tubes at the sides), there is a trio of numbers. These numbers are the Sh/Sh_{fd} values for the tube. The topmost number of each trio is for the $L^*/S = 0.8$ delivery duct, the middle number is for the $L^*/S = 2.5$ duct, and the lowermost number is for the $L^*/S = 4.5$ duct. This identification pattern is shown near the top of each figure. The specification of whether a given trio corresponds to the tube at its right or at its left will be made shortly. Figure

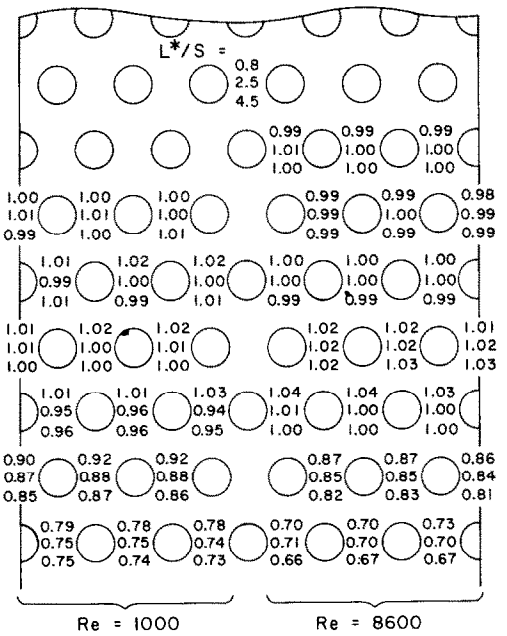

FIG. 4. Sh/Sh_{fd} values corresponding to the parallel orientation.

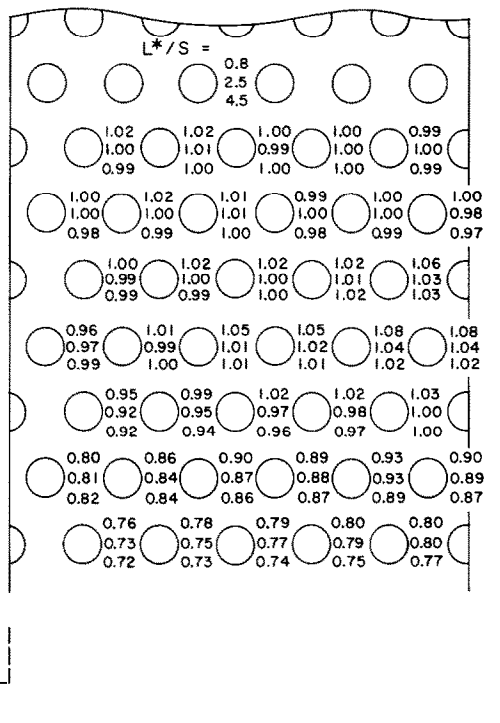

FIG. 5. Sh/Sh_{fd} values corresponding to the perpendicular orientation, Re = 1000.

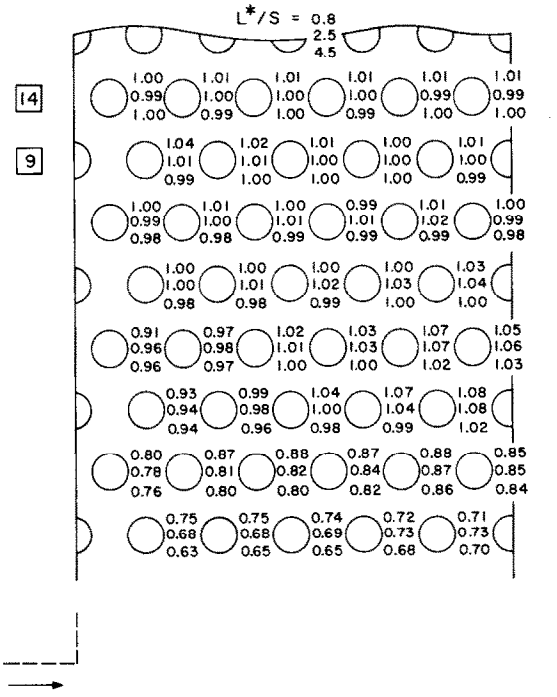

FIG. 6. Sh/Sh_{fd} values corresponding to the perpendicular orientation, Re = 8600.

Table 1. Sh/Sh_{fd} without inlet-section flow maldistribution

Row	Re 1000	Re 8600
1	0.74	0.64
2	0.86	0.83
3	0.93	~1.0
4	~1.0	

4 conveys the results for the parallel orientation, while Figs. 5 and 6 are for the perpendicular orientation. The presentation will begin with the parallel orientation.

From a consideration of Fig. 3, it is apparent that for the parallel orientation, the bend does not introduce any flow asymmetries along a given row. Therefore, in any row, symmetry should prevail with respect to a plane that is parallel to the sidewalls and situated midway between them. Advantage has been taken of this symmetry in the presentation of the results in Fig. 4. The left half of the figure contains the results for $Re = 1000$, with each trio referring to the tube at its right. In the right half of the figure are the results for $Re = 8600$. Here, each trio refers to the tube at its left.

To provide perspective for the results of Fig. 4 (as well as for Figs. 5 and 6), Table 1 conveys Sh/Sh_{fd} values for the case where the flow enters the inlet section of the tube bank without imposed maldistributions. The values listed in the table are from refs. [2, 3].

Both Fig. 4 and Table 1 confirm the well-established fact that the lowest transfer coefficients occur in the first row of the tube bank, with row-to-row increases in response to increased turbulence and mixing. One of the main points of interest in the figure is the effect of the bend-to-inlet distance L^*/S on the Sh/Sh_{fd} ratios. In the initial rows of the tube bank (rows 1–3), there is a general trend toward larger Sh/Sh_{fd} values for smaller bend-to-inlet distances. This trend is plausible in that larger disturbances should reach the tube bank from a bend that is nearer to the inlet of the bank. The variation of Sh/Sh_{fd} with L^*/S is, however, modest—8%, at most. Furthermore, beyond the third row, the Sh/Sh_{fd} ratios are insensitive to L^*/S.

It is also relevant to note that the Sh/Sh_{fd} values of Fig. 4 are within 10% of those of Table 1. Therefore, although the presence of the bend serves to enhance the mass (or heat) transfer in the initial rows, the enhancement is surprisingly small. Overall, on the basis of the present measurements, it appears that the presence of a bend installed in the parallel orientation does not require a tube-bank design procedure different from that used for the bend-free case.

Further inspection of Fig. 4 shows that the Sh/Sh_{fd} values for a given row (and at a given Reynolds number) are relatively uniform. There are no significant effects of the sidewalls in evidence.

Attention will now be turned to the Sh/Sh_{fd} results for the perpendicular orientation. Consideration of Fig. 2 suggests that for this orientation, the nonuniform flow spawned by the bend will give rise to Sherwood number variations along a given row, at least in the initial rows of the tube bundle. Therefore, the symmetry-based format used in Fig. 4 for the parallel orientation is not appropriate for the perpendicular orientation. As a consequence, the results for the perpendicular orientation are presented in Figs. 5 and 6 for $Re = 1000$ and 8600, respectively. In these figures, each trio of numbers refers to the tube at its left. As before, each number in a trio represents a value of Sh/Sh_{fd}, which, from upper to lower, corresponds to $L^*/S = 0.8$, 2.5, and 4.5. The position of the bend relative to the tube bank is illustrated schematically at the lower left of each figure.

In appraising Figs. 5 and 6, it is relevant to observe not only how Sh/Sh_{fd} at a given tube varies with L^*/S but also how Sh/Sh_{fd} varies along a row. In addition, it is appropriate to compare the Sh/Sh_{fd} values of the figures with those of Table 1 for the no-maldistribution case.

Turning first to Fig. 5 and to the results for the lower of the two Reynolds numbers, it is seen that bend-related effects are in evidence in the first five rows. At any tube in these rows, the variation of Sh/Sh_{fd} with L^*/S is, at most, about 7%—again, a rather modest effect. In general, the largest Sherwood numbers correspond to the smallest L^*/S.

At a given L^*/S, the variation of Sh/Sh_{fd} within a given row is as large as 15%, but more typical variations are 10% or less. In general, Sh/Sh_{fd} increases from left to right along a row, that is, in the direction from the inside to the outside of the bend. This trend is consistent with the packing of the flow to the outside of the bend. It is, however, surprising that the largest inter-row variations of Sh/Sh_{fd} do not occur in the first row; rather, they occur in the second row and to a slightly lesser extent in the fourth row. Also somewhat surprising is the slight dropoff which occurs at the right-hand end of the second row. All of the unexpected trends were double checked and even selectively triple checked. The check runs were always consistent to within 2% or better.

Upon comparing Fig. 5 with Table 1, it is seen that there are local bend-related enhancements as large as 10%. However, on a row-average basis, the enhancement is lower. Overall, it appears that for low Reynolds numbers ($Re \sim 1000$), the bend-related effects for the perpendicular orientation are not major.

The results corresponding to the perpendicular orientation and to the higher Reynolds number ($Re = 8600$) will now be discussed with reference to Fig. 6. Here, the main effects of the bend are confined to the first four rows, with residual effects in the fifth row and an interesting reversed maldistribution in later rows (e.g. ninth row) which will be discussed shortly. Aside from isolated sites in the first row, the variation of Sh/Sh_{fd} with L^*/S at a given tube is 10% or less. For the most part, the largest Sh/Sh_{fd} corresponds to the smallest L^*/S but with occasional exceptions.

Intra-row variations of Sh/Sh_{fd} at a given L^*/S are also in evidence. These variations are most marked in the first four rows and are greatest in the third and

fourth rows (up to 15%). In general, within a given row, Sh/Sh_{fd} increases in the direction from the inside to the outside of the bend (left to right), as expected. However, unexpectedly, the variation of Sh/Sh_{fd} along the first row for $L^*/S = 0.8$ is opposite in direction. This trend was verified by numerous check runs, and it will be illuminated by the flow visualization results. The trendwise opposite intra-row variations in the first row exaggerate the differences in Sh/Sh_{fd} with L^*/S at a given tube.

The slight dropoff at the right-hand end of the second row, already noted in Fig. 5, recurs in Fig. 6.

In row nine, for $L^*/S = 0.8$, Sh/Sh_{fd} tends to decrease (albeit slightly) from left to right. This behavior actually occurs in rows 8–11, but dies away thereafter. It is believed due to a secondary maldistribution which occurs because the flow overreaches itself as it attempts to recover from the primary maldistribution.

From a comparison of Fig. 6 with Table 1, it is seen that at certain tubes in the first row, there are bend-related enhancements of up to about 15%. However, only for the $L^*/S = 0.8$ case does the row-average enhancement approach this value. In subsequent rows, there are local enhancements as large as 8%, but the row average is hardly enhanced. Thus, for the orientation and Reynolds number in question, the effects of the bend are quite localized and do not have a major effect on the performance of the tube bank as a whole. Upon reviewing the discussion of Figs. 4 and 5, it appears that the foregoing conclusion applies to all the cases investigated here.

Pressure drop

A representative measured pressure distribution is presented in Fig. 7, where the data are for the case of the parallel orientation, $L^*/S = 4.5$, and $Re = 8600$. The ordinate displays the dimensionless pressure difference $(p_{atm} - p)/\frac{1}{2}\rho V^2$, where p_{atm} is the pressure in the ambient from which the air was drawn, and p is the local pressure. Note that $p < p_{atm}$ because the apparatus was operated in the suction mode. Consequently, increases in $(p_{atm} - p)$ correspond to a pressure drop. The quantity $\frac{1}{2}\rho V^2$ is a representative velocity head which is a constant for each case. It was evaluated as

$$\frac{1}{2}\rho V^2 = \frac{1}{2}\dot{w}^2/\rho A_{min}^2 \tag{4}$$

where ρ is the mean density in the tube bank. The value of $\frac{1}{2}\rho V^2$ from equation (4) is, strictly speaking, only appropriate for the tube bank. However, it was used throughout the entire flow circuit so that the distribution of $(p_{atm} - p)\frac{1}{2}\rho V^2$ would truly reflect the distribution of $(p_{atm} - p)$.

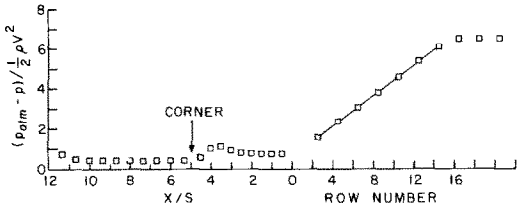

FIG. 7. Representative pressure distribution (parallel orientation, $L^*/S = 4.5$, $Re = 8600$).

On the abscissa, $X = 0$ corresponds to the inlet of the tube bank. The data for the delivery duct are plotted to the left of $X = 0$. In this range, the abscissa variable is X/S, where X is the distance from the tube bank inlet measured *upstream* along the duct centerline. To the right of $X = 0$ are the data for the tube bank and beyond. The abscissa variable in this range is the row number. Note that the last three data points correspond to pressure taps which are downstream of the tube bank, in the redevelopment duct ($S \times S$ square cross section).

At the upstream end of the delivery duct, there is a dropoff in the data (i.e. a pressure rise). This dropoff corresponds to a pressure recovery which reflects the expansion of the flow downstream of the separation caused by the sharp-edged inlet. Beyond the third pressure tap and continuing to the corner of the L, the pressure appears to be constant. Actually, there is a friction-induced pressure drop, but it is too small to be shown in the figure.

At the corner of the L, there is a pressure drop due to turning losses and separation, followed by a partial pressure recovery as the flow expands to fill the duct cross section. Thereafter, a regime of virtually uniform pressure is established, once again reflective of the extremely small friction-related pressure drop in the duct.

In the tube bank, the first pressure tap is situated midway between the second and third rows, and successive taps are separated by two rows. The data points for the tube bank fall on a straight line, suggestive of fully developed flow. Downstream of the bank, the pressure again appears to be virtually uniform.

The pressure drop Δp_{tot} for the flow circuit as a whole is of interest because it reflects the net result of differences in L^*/S and delivery duct orientation. The value of $\Delta p_{tot}/\frac{1}{2}\rho V^2$ was determined from the data at the three pressure taps situated downstream of the tube bank. Numerical values of this quantity are listed in Table 2 for all of the operating conditions of the experiments. Inspection of the table indicates that for a given Reynolds number, $\Delta p_{tot}/\frac{1}{2}\rho V^2$ is virtually independent of the delivery duct orientation and of L^*/S. Indeed, Δp_{tot} is even less sensitive to these parameters than were the Sherwood number results. This outcome is quite plausible since Δp_{tot} is an overall quantity while the Sherwood numbers were referred to individual tubes.

Table 2. Values of $\Delta p_{tot}/\frac{1}{2}\rho V^2$

		L^*/S		
Re	Orient.	0.8	2.5	4.5
1000	Par.	7.7	7.5	7.5
1000	Perp.	7.7	7.7	7.5
8600	Par.	6.4	6.4	6.5
8600	Perp.	6.4	6.5	6.5

The linear p vs X distribution in the tube bank enabled the evaluation of the fully developed friction factor for the bank. If Δp_{row} denotes the per-row pressure drop in the linear region, then the friction factor may be evaluated from

$$f_{fd} = \Delta p_{row}/\tfrac{1}{2}\rho V^2 \qquad (5)$$

where $\frac{1}{2}\rho V^2$ is from equation (4). For $Re = 1000$ and 8600, the respective f_{fd} are 0.46 and 0.36 with a scatter of $\pm 2\%$.

Flow visualization

The flow visualization work did not yield as much information as was sought. At low Reynolds numbers, the shear stresses were not large enough to move the most fluid of the oil–lampblack mixtures that were prepared. At the highest attainable Reynolds number (~ 8600), the shear stresses were of sufficient strength, but another difficulty was encountered. With the airflow activated, globules of the mixture collected at the rear of each tube and were held in place by the aerodynamic forces. When the airflow was terminated, the forces vanished and the accumulated mixture tended to spread over adjacent parts of the floor of the test section, obscuring a portion of the flow pattern traces.

For these reasons, the presentation of the flow visualization results is necessarily quite limited. Also, as noted earlier, the oil–lampblack technique, as used here, yielded information only about the flow pattern adjacent to the floor of the test section.

The flow visualization results are presented in Figs. 8(a) and (b). The white circles in these photographs correspond to the positions of the tubes. At the respective edges, the white regions are approximate half circles (difficulties in cutting the contact paper were responsible for the imperfections).

Figure 8(a) shows a typical flow pattern in the fully developed regime. As noted in the figure, the wakes from the tubes in the adjacent upstream row are deployed along the lower edge of the photograph. Between each pair of adjacent wakes is a black zone which is termed a *stagnation island* in the figure. It is relevant to note that each such island is centered directly in front of a tube. The stagnation at each island is the result of two opposing streams. One is the mainflow, which is moving in the forward direction. The second stream is a backflow which issues from the lower portion of the tube and moves upstream along the floor. Still another array of stagnation zones is in evidence in Fig. 8(a), with each zone situated just downstream of a wake. These zones are caused by the collision of two streams entering the lane between two adjacent tubes.

Attention may now be turned to Fig. 8(b). This photograph shows the first row of the tube bank for the case of the perpendicular array, $L^*/S = 0.8$, and $Re = 8600$. It may be recalled that in the discussion of Fig. 6, the first-row Sh values for this case did not increase from left to right, as was expected.

There are many differences between the flow patterns of Figs. 8(a) and (b), many of which reflect the difference between the first row and the fully developed regime. However, the altered positioning of the stagnation islands is not attributable to this. It is relevant to note that the stagnation islands in Fig. 8(b) are not located directly in front of the tubes as in Fig. 8(a) [see arrow identifying a stagnation island in Fig. 8(b)].

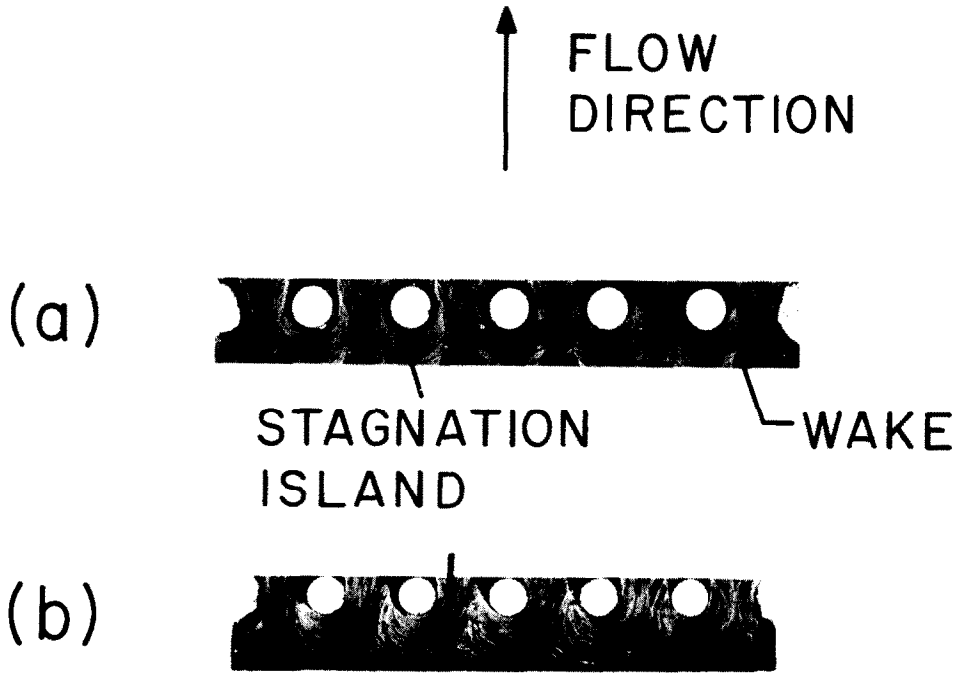

FIG. 8. Flow visualization photographs.

From the discussion in the next to last paragraph, it is clear that the position of the stagnation island tells the direction from which the fluid approaches the tube. This direction can be obtained by connecting the center of the island with the axis of the tube. Thus, relative to the nominal mainflow direction, the flow arrives at the leftmost tube of Fig. 8(b) at 45°, and the adjacent tubes also display large arrival angles.

This finding indicates that whereas the flow may have packed to the outside of the bend, by the time it reaches the first row of the tube bank it is moving diagonally in order to fill the cross section. Also, considering the sharpness of the streak lines, this diagonal flow is at least as vigorous at the left as at the right. These observations help explain the intra-row distribution of Sh/Sh_{fd} in the first row of Fig. 6 for $L^*/S = 0.8$.

CONCLUDING REMARKS

The work described here appears to be the first systematic study of the response of a heat exchanger to a right-angle bend situated upstream of the exchanger inlet cross section. Experiments were performed for a tube-bank-type crossflow heat exchanger with the tubes positioned on equilateral triangular centers with a transverse pitch-to-diameter ratio of two. The tube bank was housed in a square duct (side S), and the L-shaped duct which delivered air to the tube bank was of the same square cross section.

The effects of two geometrical parameters were investigated. One parameter is the distance L^* between the bend and the inlet of the tube bank, with the investigated values being $L^*/S = 0.8$, 2.5, and 4.5. The other geometrical parameter is the orientation of the bend in the L-shaped delivery duct with respect to the axes of the tubes in the bank. Two orientations were considered. In one, the plane of the L is parallel to the tube axes, while in the other, the plane of the L is perpendicular to the axes. For each configuration (given L^*/S and orientation), experiments were carried out for Reynolds numbers of 1000 and 8600.

For each case defined by L^*/S, orientation, and Reynolds number, the per-tube Sherwood number was measured at each relevant tube site in the array (the Sherwood number is the mass transfer counterpart of the Nusselt number). Pressure distributions were also measured along the delivery duct and the tube bank. A limited flow visualization study was also performed.

In general, it was found that the presence of the right-angle bend did not have a major effect on the heat transfer characteristics of the tube bank. For the closest proximity of the bend, individual tube transfer coefficients exceeded those for the no-bend case by 10% (in the extreme, by 15%). The departures were confined to the initial rows (first three or four rows) of the bank. Smaller bend-related effects were sustained for larger distances between the bend and the inlet of the tube bank. Row-average transfer coefficients deviated from the no-bend case by smaller percentages than the aforementioned individual tube deviations.

With the bend in the parallel orientation, there were no intra-row nonuniformities. However, the perpendicular orientation introduced intra-row variations in the transfer coefficient, with the extreme variation being 15%.

The system pressure drop (from delivery duct inlet to tube bank exit) was even less sensitive to the geometrical parameters (L^*/S and orientation) than was the per-tube transfer coefficient.

Overall, it appears that the presence of a right-angle bend does not require a tube-bank design procedure different from that for the no-bend case.

Acknowledgement—The research reported here was performed under the auspices of the Office of Naval Research.

REFERENCES

1. S. Kakac, R. K. Shah and A. E. Bergles, *Low Reynolds Number Heat Exchangers*. Hemisphere, Washington, DC (1982).
2. E. M. Sparrow and R. Ruiz, Effect of blockage-induced flow maldistribution on the heat transfer and pressure drop in a tube bank, *Trans. Am. Soc. Mech. Engrs*, Series C, *J. Heat Transfer* **104**, 691–699 (1982).
3. E. M. Sparrow and A. A. Yanezmoreno, Heat transfer in a tube bank in the presence of upstream cross-sectional enlargement, *Int. J. Heat Mass Transfer* **27**, 469–473 (1984).
4. J. P. Chiou, Thermal performance deterioration in crossflow heat exchanger due to flow nonuniformity, *Trans. Am. Soc. Mech. Engrs*, Series C, *J. Heat Transfer* **100**, 580–587 (1978).
5. A. C. Mueller, An inquiry of selected topics on heat exchanger design, Donald Q. Kern Award Lecture, 16th National Heat Transfer Conference, August (1976).
6. B. A. Dobryakov, The calculation of heat exchanger equipment with crossflow of the heat transfer agents, *Int. Chem. Engng* **13**, 81–84 (1973).
7. J. A. Kutchey and H. L. Julien, The measured influence of flow distribution on regenerator performance, SAE Trans. 83, Paper No. 740164 (1974).
8. W. Merzkirch, *Flow Visualization*, pp. 53–56. Academic Press, New York (1974).
9. H. H. Sogin, Sublimation from discs to air streams flowing normal to their surfaces, *Trans. Am. Soc. Mech. Engrs* **80**, 61–71 (1958).

ECHANGEUR DE CHALEUR SITUE EN AVAL D'UN COUDE A ANGLE DROIT

Résumé—Le transfert thermique, la perte de charge et la visualisation de l'écoulement sont étudiés expérimentalement pour un échangeur de chaleur à nappes de tubes en attaque frontale et situé en aval d'un coude à angle droit. L'échangeur de chaleur est logé dans un canal de section carrée, et le canal en forme de L qui délivre l'air à l'entrée des bancs de tubes à la même section droite. Deux paramètres géométriques sont variables au cours des expériences : (1) la distance entre le coude et la première nappe de tubes et (2) l'orientation du plan du coude par rapport aux axes des tubes (soit parallèle soit perpendiculaire aux axes). Le nombre de Reynolds varie sur un ordre de grandeur. Pour chaque géométrie et chaque nombre de Reynolds, les coefficients de transfert par tube sont déterminés pour chaque position du tube dans l'arrangement. On trouve que la présence du coude à angle droit n'a pas une grande influence sur les caractéristiques du transfert de la grappe de tube. Des accroissements liés au coude, de l'ordre de 10 à 15%, sont remarqués sur des tubes des premières nappes, mais l'accroissement global est plus faible. La non-uniformité entre nappes apparait pour l'orientation perpendiculaire mais pas pour l'orientation parallèle. La perte de pression (entre entrée du canal et sortie de l'échangeur) est moins sensible aux paramètres géométriques que le transfert thermique par tube.

ANORDNUNG EINES WÄRMEÜBERTRAGERS HINTER EINEM RECHTWINKLIGEN KRÜMMER

Zusammenfassung—An einem Kreuzstrom-Rohrbündel-Wärmeübertrager hinter einem rechtwinkligen Krümmer wurden experimentelle Untersuchungen zum Wärmeübergang, zum Druckverlust und zur Strömungsform durchgeführt. Sowohl der Kanal, in dem der Wärmeübertrager eingebautwar als auch der L-förmige Zulauf hatten denselben quadratischen Querschnitt. Bei der Durchführung der Experimente wurden zwei geometrische Parameter variiert: (1) Abstand zwischen Krümmer und Wärmeübertragereintritt, (2) Orientierung der Krümmerebene zu den Rohrachsen des Wärmeübertragers (parallel bzw. senkrecht zu den Achsen). Die Reynolds-Zahl wurde über nahezu eine Größenordnung variiert. In Abhängigkeit von Reynolds-Zahl und Geometrie wurden die Wärmeübergangskoeffizienten für die wichtigsten Rohranordnungen bestimmt. Es wurde festgestellt, daß ein rechtwinkliger Krümmer keinen wesentlichen Einfluß auf das Wärmeübertragungsverhalten des Rohrbündels hat. Verbesserungen im Bereich von 10 bis 15%, bedingt durch die Anordnung des Krümmers, konnten für einzelne Rohre im Eintrittsbereich festgestellt werden; die durchschnittlichen Verbesserungen waren jedoch geringer. Ungleichförmigkeiten ergaben sich zwischen den Reihen nur bei einer senkrechten Anordnung, jedoch nicht bei einer parallelen. Der Druckverlust des Systems (zwischen Kanaleintritt und Rohrbündelaustritt) wurde von den geometrischen Parametern noch weniger beeinflußt, als der Wärmeübergang des einzelnen Rohres.

ТЕПЛООБМЕННИК, РАСПОЛОЖЕННЫЙ ВНИЗ ПО ПОТОКУ ЗА ИЗГИБОМ ПОД ПРЯМЫМ УГЛОМ

Аннотация—Проведено экспериментальное исследование теплопереноса и падения давления, а также визуализация течения в канале с трубчатым поперечнообтекаемым теплообменником, расположенным вниз по течению за изгибом под прямым углом. Канал и *L*-образный предвключенный участок, обеспечивающие подвод воздуха к пучку труб, имели квадратное сечение. В экспериментах изменялись следующие геометрические параметры: (1) расстояние между изгибом и входом в пучок труб и (2) положение плоскости изгиба относительно осей труб пучка (параллельное или перпендикулярное). Число Рейнольдса изменялось в пределах примерно одного порядка. Для каждой геометрии и значения числа Рейнольдса коэффициенты теплопереноса отдельных труб определялись в соответствии с положением трубы в пучке. Найдено, что изгиб под прямым углом не оказывает значительного влияния на характеристики теплообмена пучка. Интенсификация в 10–15% за счет изгиба отмечалась на отдельных трубах в начальных рядах, но средняя по рядам интенсивность была ниже. Неоднородности между рядами наблюдались при перпендикулярном расположении плоскости изгиба. Падение давления в системе (от входа в *L*-образный участок до выхода из пучка труб) еще меньше зависело от геометрических параметров, чем теплоперенос от каждой трубы.